Monitoring Saturation Changes with Ambient Seismic Noise and Gravimetry in a Karst Environment

Benjamin Fores, C. Champollion, G. Mainsant, J. Albaric, A. Fort

▶ **To cite this version:**

Benjamin Fores, C. Champollion, G. Mainsant, J. Albaric, A. Fort. Monitoring Saturation Changes with Ambient Seismic Noise and Gravimetry in a Karst Environment. Vadose Zone Journal, 2018, 17 (1), 10.2136/vzj2017.09.0163 . hal-01860674

HAL Id: hal-01860674

https://hal.umontpellier.fr/hal-01860674

Submitted on 23 Nov 2021

HAL is a multi-disciplinary open access archive for the deposit and dissemination of scientific research documents, whether they are published or not. The documents may come from teaching and research institutions in France or abroad, or from public or private research centers.

L'archive ouverte pluridisciplinaire **HAL**, est destinée au dépôt et à la diffusion de documents scientifiques de niveau recherche, publiés ou non, émanant des établissements d'enseignement et de recherche français ou étrangers, des laboratoires publics ou privés.

Distributed under a Creative Commons Attribution - NonCommercial - ShareAlike 4.0 International License

Published May 3, 2018

Original Research

Core Ideas

- Saturation changes can be monitored with ambient seismic noise.
- We present a new and nondestructive tool to investigate deep and heterogeneous vadose zones.
- At the site scale, this tool fills the gap between local boreholes and global basin information.
- Different geophysical datasets can be assimilated for hydrological model calibration.

Monitoring Saturation Changes with Ambient Seismic Noise and Gravimetry in a Karst Environment

B. Fores,* C. Champollion, G. Mainsant, J. Albaric, and A. Fort

On a heterogeneous karstic site in the Larzac plateau (France), we performed cross-correlations of ambient seismic noise recorded at two broadband seismometers to obtain daily seismic velocity changes. Rayleigh velocity changes at the 6- to 8-Hz frequency band show variations of ±0.2% over 1 yr. Assuming a simple velocity profile, changes are expected to come from depths of tens of meters. Therefore velocity changes at 6 to 8 Hz were interpreted as induced by water saturation changes. A slow infiltration rate would explain the delay of several months between the rainy season (November) and the minimum velocity (June). Superconducting gravimeter, evapotranspiration, and magnetic resonance sounding (MRS) measurements were then combined with seismic data in one-dimensional physical simulations. Velocity changes clearly constrain hydrological parameters, like saturated hydraulic conductivity, even if the Biot–Gassmann theory does not explain all of the amplitude observed. Nevertheless, this nondestructive method demonstrates great potential in hydrological model calibration. It overcomes the lack of depth resolution of gravimetry and the lack of temporal resolution of MRS. The combination of ambient seismic noise with gravimetry and MRS could fill the instrumental gap currently existing in hydrology for the study of deep and/or complex critical zones.

Abbreviations: AET, actual evapotranspiration; GEK, Geodesy in Karstic Environment observatory; KGE, Kling–Gupta efficiency; MRS, magnetic resonance sounding; MWCS, moving-window cross-spectrum analysis; PET, potential evapotranspiration.

B. Fores, C. Champollion, and A. Fort, Géosciences Montpellier, CNRS, Univ. Montpellier, UA, Montpellier, France; G. Mainsant, Lab. de Planétologie et Géodynamique, CNRS, Univ. Nantes, Nantes, France; J. Albaric, Chrono-environnement, CNRS, Univ. Bourgogne Franche-Comté, Besançon, France. *Corresponding author (benjamin.fores@gm.univ-montp2.fr).

Received 4 Sept. 2017.
Accepted 7 Mar. 2018.

Citation: Fores, B., C. Champollion, G. Mainsant, J. Albaric, and A. Fort. 2018. Monitoring saturation changes with ambient seismic noise and gravimetry in a karst environment. Vadose Zone J. 17:170163. doi:10.2136/vzj2017.09.0163

© Soil Science Society of America. This is an open access article distributed under the CC BY-NC-ND license (http://creativecommons.org/licenses/by-nc-nd/4.0/).

For several years, interest has been growing for modeling processes in the critical zone, as demonstrated by the increasing number of dedicated national programs all around the world (Brantley et al., 2015). The critical zone includes the vadose zone, where flows are ruled by complex relations depending on saturation, and may spatially vary strongly because of heterogeneities, possible clayey material, or fractures. Despite this heterogeneity, many studies have focused on core samples or on moisture probes to estimate the hydraulic properties at variable saturations. However, small-scale properties derived from these studies are not representative of whole sites on heterogeneous systems such as karsts. Moreover, hydrological tools such as piezometers are local and unsuitable because they are sensitive only to water table changes. The same problem is encountered for thick vadose zones where water tables are too deep to be measured and where tools like neutron probes are too shallow. Currently, measuring instruments are missing to estimate an averaged hydraulic conductivity representative at the field scale (100 m) on a thick and locally heterogeneous vadose zone. This is preventing spatialized modeling, knowledge transfer, and vulnerability assessment or mapping.

Various geophysical methods are already used for hydrological modeling, but they all have limitations that seismic monitoring may circumnavigate because it is an integrative method on a defined depth range depending on the frequency. Gravimetry has been used in recent studies on heterogeneous media, in different contexts, because it directly measures water content variation at a large scale, averaging small heterogeneities (Jacob et al., 2008; Pfeffer et al., 2013; Fores et al., 2017a; Güntner et al., 2017). Gravimetry is also useful for focused infiltration (e.g., Kennedy et al. 2014), but one drawback of this averaging property is that gravimetry lacks depth resolution for one-dimensional infiltration. Considering infinite horizontal slabs (i.e., a tabular model), a given amount of water has exactly the same

attraction effect on a gravimeter, regardless of depth and porosity. Magnetic resonance sounding (MRS) (Legchenko and Valla, 2002; Chalikakis et al., 2011) is another integrative method that directly provides water content at depth and has already been successfully applied to locally heterogeneous karstic media (Mazzilli et al., 2016). However, it lacks time resolution and is not yet designed for monitoring. In this study, we combined accurate continuous gravity signals and MRS water content profiles with daily seismic velocity changes obtained from the correlation of ambient seismic noise.

Our goal was to investigate the potential of seismic monitoring, which would allow retrieval of seismic velocity changes, to complete and overcome lack of depth resolution of gravimetry and the lack of temporal resolution of MRS. Hydrologic models and seismic velocity changes are linked by the dependence of the seismic velocity on the density of the medium, in this case water content. The depth sensitivity of the method comes from the dispersive property of the surface waves, and the passivity of the method allows for continuous time series. The ambient noise correlation technique has developed quickly in the last decade and offers a realistic alternative to controlled sources (Campillo and Paul, 2003). Changes in the medium can be assessed through apparent velocity variation, which can be measured with a precision much greater than 0.1% (Sens-Schönfelder and Wegler, 2006; Brenguier et al., 2008b). Although numerous studies have interpreted velocity changes as hydrologically induced signals, few have focused on them (Sens-Schönfelder and Wegler, 2006; Voisin et al., 2016; Lecocq et al., 2017), and no ambient seismic noise experiments were originally designed for hydrology. The question we tried to answer in this study is: Can we use ambient seismic noise as a timer to follow water infiltration in deep unsaturated media at the field scale, integrating a radius of hundreds of meters?

Site Overview

Local Hydrogeological Settings

The studied site is the Geodesy in Karstic Environment (GEK) observatory surroundings, on the Durzon karstic basin (Larzac, south of France). The basin is made of highly weathered dolostones, and the site topography is quite flat (around 700 m asl; Fig. 1). The only spring is located 5 km away at an altitude of 533 m asl, that is to say 170 m lower than the observatory altitude. The unsaturated zone is at least 100 m thick on the site. Indeed, crawlable dry caves are found beneath the site at 600 m asl, giving a minimum limit for the unsaturated zone thickness at the field scale. However, perched aquifers can exist above the caves, in the uppermost and weathered part of the unsaturated zone of a karst, called the *epikarst* (Williams, 2008). The epikarst plays a key role in water storage in the Durzon basin. Actually, hydrological, hydrochemical, and gravity monitoring indicate a well-developed epikarstic storage zone at the whole karst system scale (110 km^2; Jacob et al., 2008, and references therein).

Geophysical Background at the Observatory

Epikarstic storage is also demonstrated at the site scale from borehole measurements and several geophysical studies. Three boreholes (up to −50 m) located close to the observatory (Fig. 1) reveal high macroporosity (around 10%) without any fractures. Boreholes also highlight the strong horizontal and vertical heterogeneity at small scales, which is typical of karstic media (e.g., Jazayeri Noushabadi et al., 2011). Indeed, the three boreholes show different water tables and a dolomite alteration varying widely along the vertical (Mazzilli et al., 2016).

Since 2011, the observatory has been equipped with two rain gauges, a flux tower to ensure accurate actual evapotranspiration (AET) measurements, and a superconducting gravimeter (iGrav #002). Local hydrological gravity residuals were computed with a classic approach (Hinderer et al., 1991), which includes the reduction for Earth tides, ocean and global hydrological loadings, barometric pressure variations, polar motion, and instrumental drift. The method description for this specific iGrav can be found in Fores et al. (2017a, supplementary material). Gravity residuals are very well correlated with modeled water storage changes using precise measurements of AET and precipitation. A

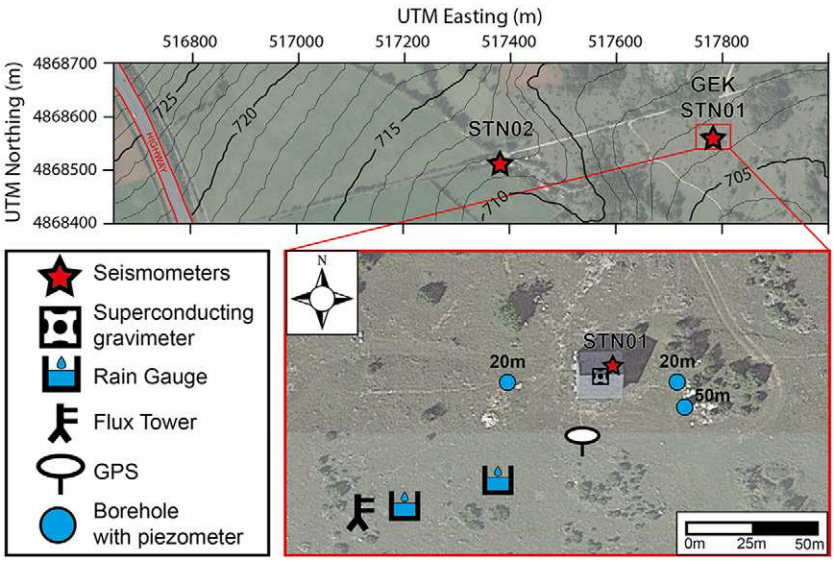

Fig. 1. Geodesy in Karstic Environment (GEK) observatory setup: large view of the site with 1-m-height contour levels (top) and close-up of the observatory and close surroundings (bottom).

constant local water output of ~1 mm d^{-1} at depth was inferred, without any faster transfer even during high-precipitation events (Fig. 2). Despite the local heterogeneity revealed by boreholes, gravimetry studies have shown that the site can be considered as a one-dimensional tabular model without a significant fast transfer at the hectare scale due to the inherent integrative characteristic of the gravity scale (Fores et al., 2017a; 2017b).

Magnetic resonance soundings were performed four times prior to the observatory building and at its exact location in July 2009, April 2010, May 2010, and May 2011 by Mazzilli et al. (2016, H3 site). The MRS revealed that water content increases with depth, with some temporal changes in the upper part, while it is stationary (8% at the resolution of the sounding) below 20 m (Fig. 2c). Note that we consider the decrease in MRS water content after 35 m insignificant because it is not corroborated by water content or porosity from core samples (from the 50-m-deep borehole) and because of MRS loss of resolution with depth. Then both MRS and gravity monitoring demonstrate that the upper part of the karst is one of the major storage zones.

Passive Seismic Monitoring

Principle

Classically, the impulse response (or Green function) is retrieved by active ways. A source signal is emitted at a given point and is recorded by a seismic sensor at another point. Developments in acoustic (Weaver and Lobkis, 2001) and seismology (Campillo and Paul, 2003) showed that the local Green function can be determined from cross-correlation of ambient seismic noise continuously recorded by two passive sensors. In other words, this function is similar to a seismogram recorded at one of the two receivers, while the second one would be the location of an active source. The continuity of the records allows monitoring relative seismic velocity variations (d*V*/*V*) by comparing correlograms with time and thus monitoring changes in the seismic properties of the medium. To obtain d*V*/*V*, a complete Green's function does not necessarily need to be rebuilt, and correlograms are only required to be stable in time, implying a relatively constant background noise during the period of interest (Hadziioannou et al., 2009). It is preferable to use the tail portion of the correlograms formed by scattered waves (the so-called *coda* part), rather than first arrivals, which are very sensitive to change in the noise source position (Poupinet et al., 1984; Snieder et al., 2002). Coda waves follow long and scattered paths and are sensitive to small variations in the seismic properties of the medium (Poupinet et al., 1984; Brenguier et al., 2008a; Hadziioannou et al., 2009).The error in d*V*/*V* may be less than 0.1% (Sens-Schönfelder and Wegler, 2006; Brenguier et al., 2008a).

Data Acquisition and Processing

To monitor seismic velocity changes in the medium, two seismometers were installed from October 2014 to November 2015 (Fig. 1). Both seismometers recorded the three components at a 250-Hz sampling frequency. Seismometer STN01 (an STS-2, Kinemetrics) was set inside the observatory on a concrete pillar. Seismometer STN02 (a Trillium compact, Nanometrics) was set 400 m away in a private individual's basement, dug in the base rock and then directly in contact with dolostones. Both were connected to a Taurus (Nanometrics) datalogger.

Signals were studied in the 1- to 20-Hz frequency range. Below 1 Hz, the level of noise is strong and related to marine swell (Fig. 3b). At higher frequencies, clear day/night and week/weekend patterns reveal the anthropic origin of the noise (Fig. 3a). Above 10 Hz, a constant and high noise level is observed about every 1 Hz and attributed to electronic noise produced by other instruments in the observatory. To determine the source direction, we calculated Fourier spectra from the north and east components for each azimuth at 1° angular increments to display the spectral content of ambient vibrations in the horizontal plane (Bottelin et al., 2013). The 8- to 15-Hz noise polar plots show a southwest–northeast direction (Fig. 3c), which is consistent with traffic on the highway located

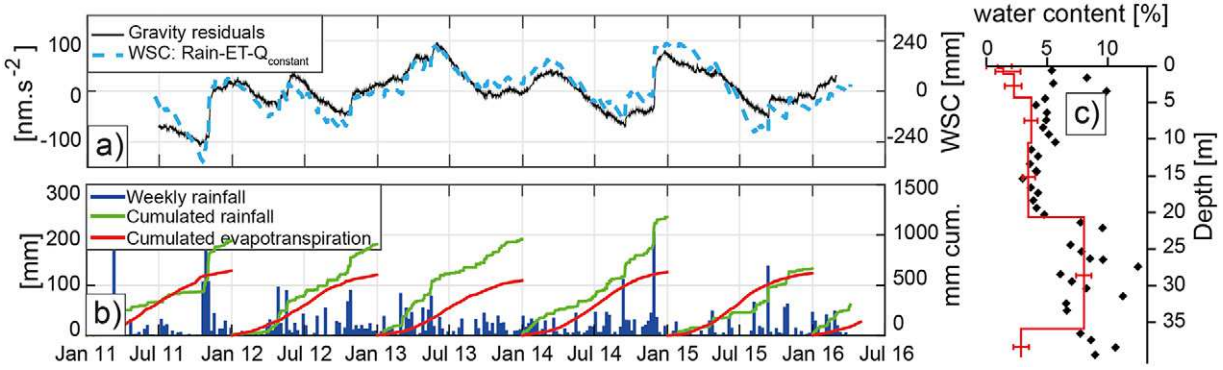

Fig. 2. Geophysical background at the Geodesy in Karstic Environment (GEK) observatory: (a) gravity residuals from the iGrav superconducting gravimeter from Fores et al. (2017a), with the height variations of an equivalent infinite horizontal water slab on the right axis and simple water storage changes (WSC) computed (blue dotted line) from precipitation and evapotranspiration (ET) measurements and a constant output (Q) of 1 mm d^{-1}; (b) weekly rainfall (blue bars) and yearly cumulated rainfall and evapotranspiration (green and red lines, respectively); and (c) magnetic resonance sounding (MRS) water content (red line) and core sample water contents (markers) from Mazzilli et al. (2016).

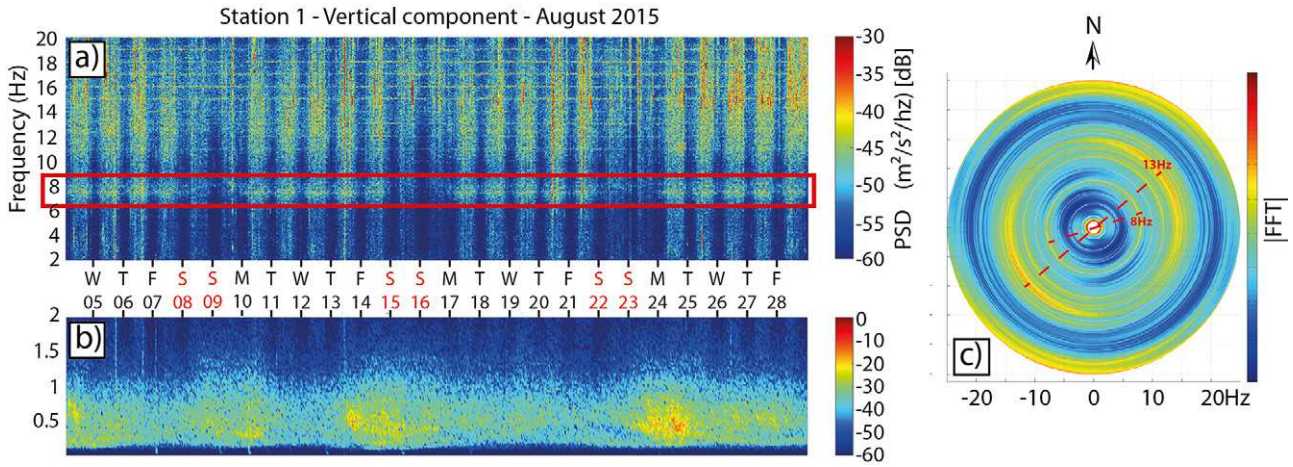

Fig. 3. An STN01 spectrogram for August 2015 (a) between 2 and 20 Hz and (b) below 2 Hz, along with (c) an azimuthal diagram. Because of its symmetry, this diagram provides only an orientation.

southwest of both sensors (Fig. 1). Although the traffic is not stable in the short term, it statistically stabilizes when averaged across a day (Mainsant et al., 2012).

From Cross-Correlation Functions to Velocity Changes

Cross-correlation functions and dV/V have been computed from the vertical component and for different frequency bands using the MSNoise software (Lecocq et al., 2014) based on the moving-window cross-spectrum analysis (MWCS) method (Ratdomopurbo and Poupinet; 1995, Clarke et al., 2011). The main idea is to measure the time shift between two different signals (two cross-correlation functions) in small time windows, each centered at a different time t. The delay dt vs. t is obtained by repeating the procedure at different times t along the two signals. At last, dV/V is simply the opposite of the slope: $\mathrm{d}V/V = -\mathrm{d}t/t$ (Hadziioannou et al., 2009). Another way to measure dV/V is the stretching technique, which consists in testing several possible velocity changes dV/V by resampling the correlograms in time and then taking the one that maximizes the correlation coefficient (Sens-Schönfelder and Wegler, 2006). This method was also applied and confirmed the MWCS results.

The MSNoise process includes instrumental response correction, resampling, whitening, filtering, computations of the cross-correlation function for each day and for the whole year of measurements (the reference cross-correlation function), and finally the estimation of dV/V. The final precision can be enhanced either by increasing the number of days stacked together before the estimation of dV/V or by stacking several dV/V values obtained from different pairs of seismometers. In this study, a 7-d stacking showed improvements as we had only one pair of seismometers and a source showing a weekly pattern. The MWCS was performed on a [−5,−1] s and [1,5] s time lag to avoid ballistic waves (Sens-Schönfelder and Wegler, 2006) and with a minimum coherence of 0.85 on the delay measurement (dt) between the reference and the current cross-correlation function.

Results

Seismic velocity changes are shown in Fig. 4. Relative phase velocity changes were analyzed from 1 to 20 Hz. Coherent results were obtained around 1 Hz and for the 6- to 8-Hz frequency band, using the whole year as reference (Fig. 4a). While the dV/V at 1 Hz is constant with time (red line), the 6- to 8-Hz band shows a unique cycle over 1 yr (black line), with an amplitude of 0.4% and a minimum in June 2015. At higher frequencies, results are unsatisfactory, which is most likely due to the high level of electronic noise (Fig. 3a).

Interpretation of Relative Seismic Velocity Variations

Depth of Velocity Changes

It is commonly assumed that Rayleigh waves (R-waves) are reconstructed by correlating the ambient seismic noise because they carry most of the energy on the vertical component (e.g., Mainsant et al., 2012). To interpret dV/V in terms of depths of changes, R-wave sensitivity, which depends on frequency, must be evaluated assuming a one-dimensional medium. Sensitivity profiles were computed using the software developed by Herrmann (2013) for a two-layer profile with a 1-m discretization interval (Fig. 4c). Motivations for choosing this model are described in more detail below because it was also used to match the HYDRUS numerical model. The S-velocities were based on active seismic survey. Surface wave inversion shows a first slow layer (400 m s^{-1}) in the first meters, followed by velocities around 1000 m s^{-1}. The P-wave velocities (V_P) were computed from the S-wave velocities (V_S) with a Poisson coefficient of 0.33. Density and porosity were set to 2550 kg m^{-3} and 10%, respectively, from core sample measurements and previous surface-to-depth gravity measurements in the Durzon dolostones (e.g., Jacob et al., 2009). The profile has been simplified as shown in Table 1.

Using this velocity model, we observed that a 1-Hz R-wave is almost insensitive for the first hundred meters (Fig. 4c, red line).

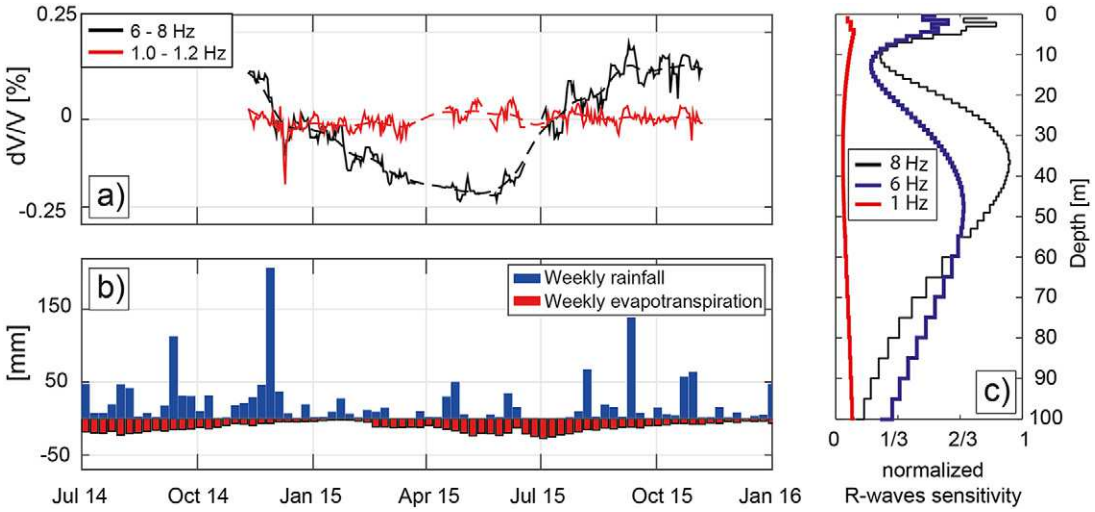

Fig. 4. (a) Seismic velocity changes (dV/V) using ambient seismic noise, after a band-pass filtering at 1 to 1.2 Hz (black line) and 6 to 8 Hz (red line); (b) weekly rainfall and evapotranspiration between July 2014 and January 2016; and (c) sensitivity kernel at 1, 6, and 8 Hz computed by the software developed by Herrmann (2013). Sensitivity is the partial derivative of R-waves phase velocity ∂_C with respect to the S-wave velocity B (∂_C/∂_B).

Therefore, the absence of velocity variations at 1 to 1.2 Hz (Fig. 4a, red line) is consistent with hydrological conditions, which are not expected to change below the 100-m depth. On the contrary, 6 and 8 Hz correspond to R-wave penetration depths of several tens of meters. Two peaks of R-wave sensitivity are visible at these frequencies (Fig. 4a, blue and black lines). The maximum sensitivity is at 35 m (8 Hz) or 45 m (6 Hz), and the area between 20 and 60 m represents 60% of the total sensitivity for the first 100 m at 8 Hz. We observe another peak close to the surface, having a lower integral value (11% at 8 Hz). It is most likely induced by the shallow slow velocity layer. Consequently, saturation changes at the depths of great sensitivity (0–10 and 20–60 m) result in large dV/V in the 6- and 8-Hz bands. From the 10- to 20-m depth, changes in water content have little effect on dV/V. Discrimination of the two sensitive areas for the origin of dV/V can be achieved through the response time, in the case of episodic rainfalls, or through modeling.

Saturation Changes

We want to have a first idea of the order of magnitude of the saturation changes needed to explain the dV/V. Many active seismic studies quantify the effect of saturation changes on seismic velocities (e.g., Adelinet et al., 2018; Galibert, 2016; Pasquet et al. 2015, 2016a, 2016b). The petrophysical relationship between hydrological properties and seismic velocities is rather complex, but R-wave velocities (V_R) mainly depend on S-wave velocities (V_S). The V_S changes with water saturation (S) were evaluated using the Biot–Gassmann relation for consolidated material (i.e., constant shear modulus with saturation; Biot, 1956a, 1956b; Gassmann, 1951). Given that

$$V_S = \sqrt{\frac{\mu}{\rho}} \qquad [1]$$

with

$$\begin{cases} \mu(S) = \mu \\ \rho(S) = \rho_{min}(1-\phi) + \rho_w(\phi S) + \rho_{air}\phi(1-S) \end{cases} \qquad [2]$$

where μ is the shear modulus; ρ is the bulk rock density; ρ_{min}, ρ_w, and ρ_{air} are the density of rock minerals, water, and air, set to 2800, 1000, and $\sim$0 kg m^{-3}; S is the saturation; and ϕ is the porosity. Neglecting the air density, we obtain from Eq. [1] and [2] the following quasi-linear relation between V_S and S:

$$V_S(S) = V_{S,dry}\left\{1 - S\left[1 - \sqrt{\frac{\rho_{min}(1-\phi)}{\rho_{min}(1-\phi)+\rho_w\phi}}\right]\right\} \qquad [3]$$

where $V_{S,dry}$ is the velocity of dry rock (S = 0). Assuming a mean porosity of 0.1 (the value observed in core samples) and a 100% saturation increase, Eq. [3] gives a V_S decreasing by about 2%. Then the dV/V of 0.4% observed at 6 to 8 Hz could be explained by a saturation change of 20%. It is important to remember that this represents only the global change across the most sensitive depths, between 20 and 60 m.

Hydrological Implications

The observed dV/V changes are consistent with meteorological measurements: dV/V decreases after rainfalls, i.e., when the saturation increases (Eq. [3]). The potential saturation range of

Table 1. Profile used to compute Rayleigh wave sensitivities.

Layer	Depth	S-wave velocity	P-wave velocity	Density	Porosity
	m	m s^{-1}		kg m^{-3}	%
1	0–5	400	800	2550	10
2	5–∞	1000	2000	2550	10

variation is around 10%, which is realistic. In addition, it is not necessarily contradictory with the constant MRS water content of 8% at this depth (Fig. 2c). Indeed, the uncertainty of ±0.7% on MRS water content allows saturation changes of ±7% for a porosity of 0.1. Consequently, it is very likely that the dV/V signal at 6 to 8 Hz is hydrologic and the single cycle of variations is due to the unique major rain event this year.

The dV/V minimum is several months delayed compared with the main rainfall event (November 2014, Fig. 4b). If we assume that this major event was the pulse initiating the dV/V decrease, it would imply a very slow advancement of the wetting front toward the sensitive area, which is deep regarding the sensitivity at 6 to 8 Hz. This 6-mo delay and the maximum sensitivity between 35 and 45 m give us a rough estimate of the advancement of the wetting front at 20 cm d^{-1}. The 6- to 8-Hz R-waves are also sensitive to the first layer (0–5 m), which is significantly slower (400 compared with 1000 m s^{-1}, Table 1). Then some short-term variations may be due to saturation changes at the near surface, immediately after rainfall (November 2014, 200 mm; September 2015, 140 mm) or with the start of the summer evapotranspiration (June 2015). However, some variations having comparable amplitude are obviously noise and should not be mistaken for hydrological signals. Note that we use the same frequency band as Voisin et al. (2016), who found hydrologically induced dV/V constrained in the 6- to 8-Hz band from the analysis of a similar source of ambient seismic noise (traffic) but in a different context: a very slow porous medium and consequently shallow investigation depths.

From these encouraging results, we next combined all geophysical signals in one simple hydrological model to confirm their complementarity, reproducing (i) the total unsaturated zone storage changes from gravimetry, (ii) the delayed saturation changes in depth from passive seismic, and (iii) the average MRS water content value around which the saturation changes took place.

Assimilation in a One-Dimensional, Numerical, Physically Based Model

Hydrological Model Definition

The choice of representing the heterogeneous epikarst by an equivalent one-dimensional model at the geophysical measurement scale was supported by previous studies, as mentioned above. We followed the principle of parsimony and defined a simple two-layer model, associated with only a minimum of parameters for the inversion. Hydrological simulations were performed using the HYDRUS-1D software (Šimůnek et al., 2008, 2016) dedicated to one-dimensional flow simulations in unsaturated porous media. This software solves the van Genuchten head-based solution (van Genuchten, 1980) of the Richards equation (Richards, 1931). Fracture flows were not added to the model because gravimetry did not show significant fast transfer. Moreover, at a smaller scale, no fractures were observed in the boreholes.

Models were run with variable time steps and a warming stage starting in 2004. The finite-element mesh divides the profile into linear elements. The spacing between the nodes forming the element corners increases with depth, with a maximum increase factor of 1.5 (Šimůnek et al., 2008). Two materials and 1001 nodes represent the medium (Fig. 5). The model is consistent with the seismic velocity profile defined in Table 1. We defined a first layer of soil (0–5-m depth), which is necessary to accommodate rainfall without creating runoff (never seen on the site). A second layer was set from the 5-m depth to the base of the model, at the 100-m depth. It represents the unsaturated zone, which is characterized by high secondary porosity (i.e., porosity created through alteration of rock) and distributed water at the gravity scale. Boundary conditions at the surface were rainfall and potential evapotranspiration (PET). HYDRUS-1D adapts the PET depending on shallow water availability. A constant flux of 1 mm d^{-1} was defined as the bottom boundary condition, as determined from the gravity-driven water mass balance. On the

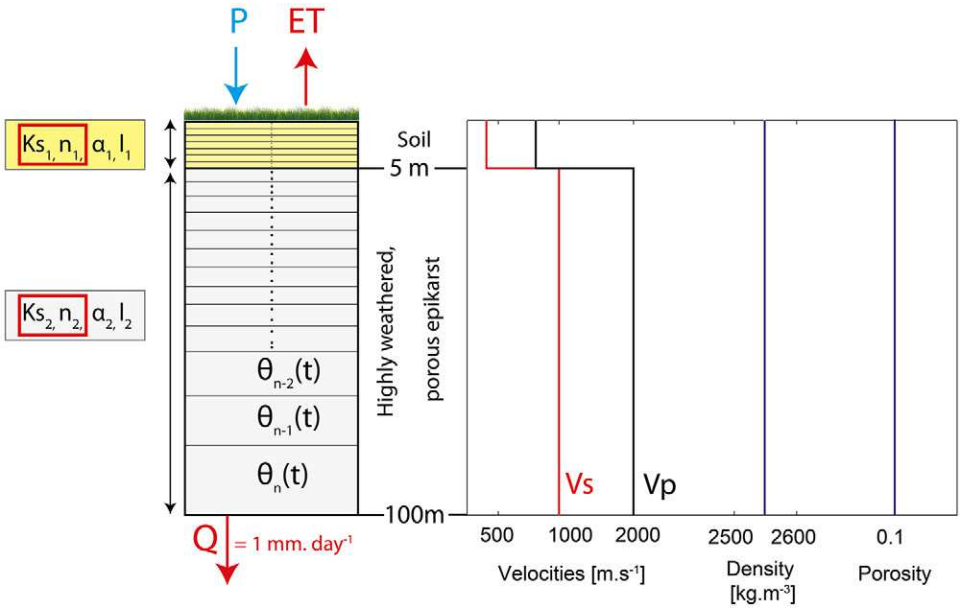

Fig. 5. Scheme of the two-layer hydrological model with node spacing increasing with depth, P-wave and S-wave velocity (V_P and V_S) profiles, and density and porosity profiles. Inputs of the hydrological model are precipitation (P) and potential evapotranspiration (ET). A constant bottom flux Q of 1 mm d^{-1} is set from gravity-driven mass balances; $\theta_i(t)$ is the water content of the ith element of the model at a time step t; and K_s, n, α, and l are the van Genuchten parameters. Only K_s and n in the two layers were researched during the inversion.

GEK site, 50 m is a minimum model size because core samples show weathered dolostones down to this depth. For this first approach, we assumed that the porous medium continues down to the dry caves, 100 m underneath the GEK observatory.

Simulated Gravity Changes

Simulated gravity is calculated from the sum of the water content of each element of the HYDRUS model using the infinite slab model (e.g., Jacob et al., 2008), as we assume a one-dimensional model and uniform recharge. A building mask effect on rainfall (Deville et al., 2012) can be used to estimate the first-layer parameters. It is taken into account through a coefficient C depending on depth and set from direct modeling (Fores et al., 2017a):

$$g_c(t) = \sum_{i=1}^{n} 2\pi\rho_w G\theta_i(t) h_i C_i \quad [4]$$

where $g_c(t)$ is the computed gravity at a time step t, G is the universal gravity constant (6.61×10^{-11} m^3 kg^{-1} s^{-2}), ρ_w is the density of water (1000 kg m^{-3}), and θ_i is the water content of the ith element of size h_i of the model.

Simulated Relative Seismic Velocity Variations

The S-wave velocity dry profile was defined following Table 1. For each day, the V_S profile is slightly changed using the 7-d mean saturation output of the hydrological model (to match the 7-d cross-correlation stacking) and using Eq. [3]. A reference profile was also calculated for the mean saturation of the whole period, which is the reference used to get the experimental dV/V. The P-wave velocities were not recomputed because they have less impact on R-waves, but we will discuss the consequences of this simplification below. For simplicity, the observed 6- to 8-Hz phase R-wave velocity changes were compared with simulations at 8 Hz. The phase velocity at 8 Hz was then computed for each day [$V(t)$] and for the whole period (the velocity reference V_{ref}) using the software developed by Herrmann (2013). Finally, we computed dV/V for each day:

$$\frac{dV}{V} = \frac{V(t) - V_{ref}}{V_{ref}} \quad [5]$$

Optimization

The van Genuchten solution (van Genuchten, 1980) uses four parameters to describe the water content and hydraulic conductivity evolution with head pressure (Fig. 5). Saturated water content (θ_s) is involved, as well as saturated hydraulic conductivity (K_s) and three parameters: n, α_{VG}, and l (in order of importance). All these parameters cannot be determined with only one dV/V signal (6–8 Hz) and a single year of data. Only n and K_s were optimized, for both layers, using a neighborhood algorithm (Sambridge, 1999). The search ranges are given in Table 2. The value of θ_s was set to 0.10 using the porosity estimation (Table 1). The values of l and α_{VG} were set to 1.5 and 0.5, respectively, which are the mean values for many rocks (Mualem, 1976) but are purely hypothetical for our karstic site. Our main objective in this study was more to show the potential of dV/V measurements for calibrating hydrological parameters of the vadose zone than to obtain their real values for this site.

Table 2. Research ranges and results for the parameter saturated hydraulic conductivity (K_s) and the shape parameter n for the first and second layers.

Parameter	K_{s1}	n_1	K_{s2}	n_2
	m d^{-1}		m d^{-1}	
Range	1–10,000	>1–2.5	0.01–100	>1–2.5
Optimization on all datasets	17.25	1.32	0.11	1.27

The objective function of the inversion was the maximization of a combination of the Kling–Gupta efficiency (KGE; Gupta et al., 2009) between observed and simulated data:

$$KGE = 1 - \sqrt{\left[S_r(r-1)^2\right] + \left[S_\alpha(\alpha-1)^2\right] + \left[S_\beta(\beta-1)^2\right]} \quad [6]$$

with

$$r = \frac{\sigma_{os}}{\sigma_o \sigma_s} \quad [7]$$

$$\alpha = \frac{\sigma_s}{\sigma_o} \quad [8]$$

$$\beta = \frac{\mu_s}{\mu_o} \quad [9]$$

The KGE is a normalized root mean square that explicitly separates the contribution of the linear correlation coefficient (r, Eq. [7]), variability (α, Eq. [8]), and bias (β, Eq. [9]) between observed and simulated data in the misfit. All of them are weighted with coefficients (S_α, S_β, S_r), while (μ_s, σ_s) and (μ_o, σ_o) are the means and standard deviations of the simulated and observed data, respectively, and σ_{os} is their covariance.

Four KGEs were computed separately, one for each data type: gravity ($KGE_{gravity}$), AET (KGE_{ET}), dV/V ($KGE_{dV/V}$), and the mean water content between 20 and 40 m (KGE_{wc}). The contribution of α, β, and r for each KGE were defined as follows: for AET, variability, bias, and r were involved ($S_\alpha = 1$, $S_\beta = 1$, $S_r = 1$). Because observed gravity changes are only relative changes, bias was not involved in the KGE between observed and simulated gravity ($S_\alpha = 1$, $S_\beta = 0$, $S_r = 1$). This amounts to setting the mean observed gravity equal to the mean simulated gravity. For dV/V, variability was not included because we were not able to reproduce the amplitude of the observed signal ($S_\alpha = 0$, $S_\beta = 1$, $S_r = 1$). Several possible reasons are discussed below. Finally, we looked only at the bias between the simulated mean value water content between 20 and 40 m and the observed 8% MRS, as it is a single value ($KGE_{wc} = \beta$). The optimization with the neighborhood algorithm (Sambridge, 1999) was performed on a combined objective function, KGE_{combi}:

$$KGE_{combi} = \frac{w_{gravity}KGE_{gravity} + w_{ET}KGE_{ET} + w_{dV/V}KGE_{dV/V} + w_{wc}KGE_{wc}}{w_{gravity} + w_{ET} + w_{dV/V} + w_{wc}} \quad [10]$$

where $w_{gravity}$, w_{ET}, $w_{dV/V}$, and w_{wc} are the weights applied to the separate KGEs, 1 or 0. Then the combined KGE is the arithmetic mean of the KGEs of the datasets we want to take into account. Finally, the neighborhood algorithm was run several times with different random seeds (Sambridge, 1999) to avoid local minima.

Inversion Results

Figure 6 presents the results depending on which datasets were used in the optimization. Gravity and AET were always included in the objective function because they define the mass balance ($w_{gravity}$ = 1 and w_{ET} = 1, Eq. [10]). Note that gravity changes are sensitive to groundwater storage changes, already known from the bottom boundary flux, AET, and rainfalls. However, including gravity in the objective function, and not only AET, remains valuable. Indeed, it allows automatic selection of models with a small numerical water budget error on the instrumented period only, without considering the warming stage. Consequently, it is not surprising that gravity is always well reproduced (KGE > 0.88, Fig. 6a). The small differences between observed and simulated gravity are mainly due to hydraulic conductivity in the first layer and the recovery of the building mask effect, then only the very short-term gravity response. We can also note that for the coupled inversion of all datasets, the mean water content between 20 and 40 m was well reproduced to match the 8% measured by MRS (Fig. 6d). Simulated water content changes at these depths stand in the error bars of the MRS measurement, which could explain why the water content has been seen to be constant for three surveys over 2 yr (Mazzilli et al., 2016).

However, the dV/V amplitude of 0.4% was not reproducible with our simple model. This issue is not caused by the assimilation of the MRS water content, which constrains the water content changes to occur around a saturation of 80%. Indeed, dV/V is not larger when MRS is not taken into account during the inversion. The long delay between the rainfall and the minimum dV/V requires a slow infiltration rate that induces too weak saturation changes at depth (20–60 m). The V_S changes from Biot–Gassman theory do not induce a dV/V of 0.4%, once weighted by the sensitivity at 8 Hz. Possible reasons are discussed below. Consequently, we tried only to reproduce the shape of dV/V: the weight of the variability between observed and simulated dV/V was weighted to 0 to compute $KGE_{dV/V}$ (S_α = 0, Eq. [6]). It means that we only searched for a linear relation between saturation and V_S. In that case, it was possible to fairly reproduce the dV/V signal (Fig. 6b) but with a linear coefficient equaling six to seven times the one calculated from Biot–Gassmann relations (Eq. [3]).

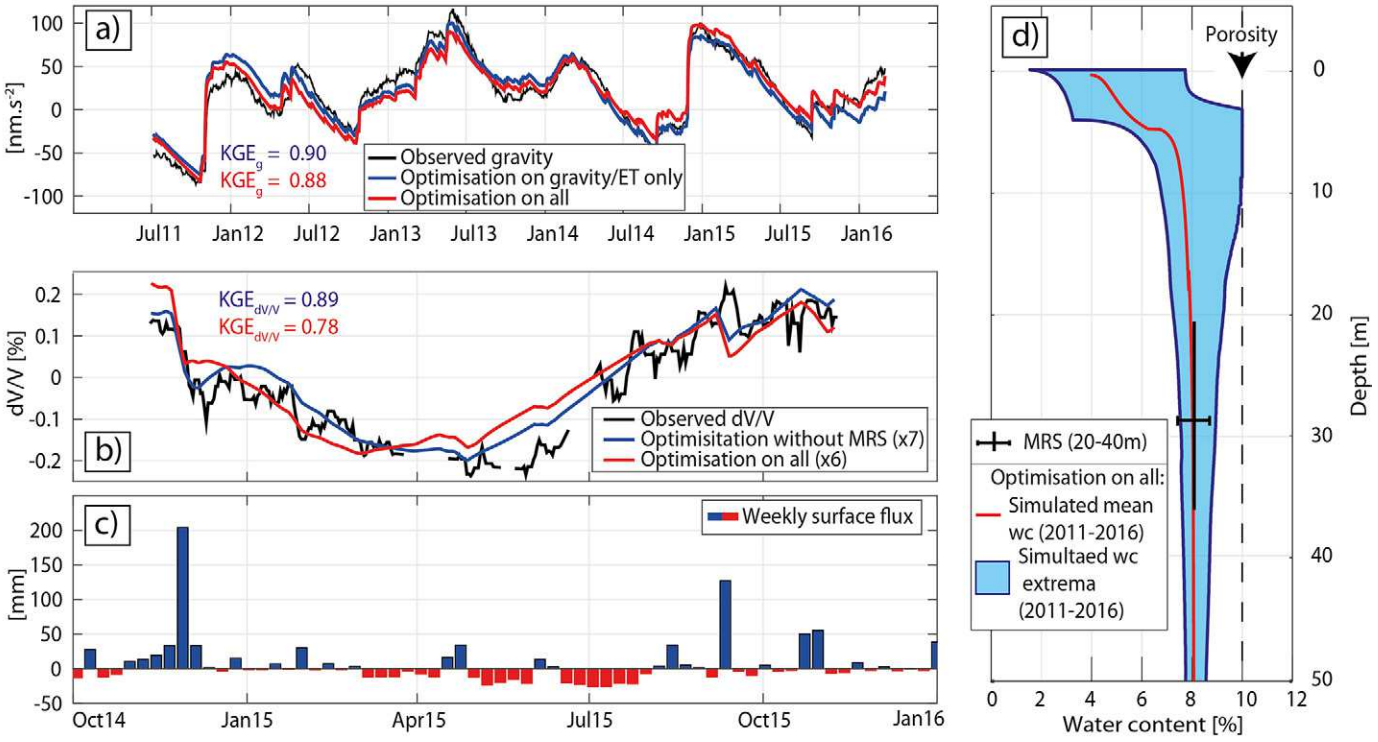

Fig. 6. Modeling results and Kling–Gupta efficiencies (KGEs): (a) observed and simulated gravity when the model parameters were searched to reproduce only observed actual evapotranspiration (AET) and gravity (blue line) or AET, gravity, relative seismic velocity variations (dV/V), and magnetic resonance sounding (MRS) mean water content (red line), with the means of simulated and observed gravity both set to zero to compare only gravity changes with time and not relative to an initial condition; (b) observed (6–8 Hz) and simulated (8 Hz) dV/V when the model parameters were searched to reproduce AET, gravity, and dV/V (blue line), plus MRS (red line); (c) weekly observed surface flux (rainfall minus AET); and (d) water content (wc) measured by MRS between 20 and 40 m (in black, from Mazzilli et al., 2016), mean simulated water content (in red), and simulated water content extrema (in blue), with the simulated dV/V amplified by 7 and 6.

Short-term observed dV/V signals are mainly noise, but some dV/V decreases are possibly induced by precipitation. Indeed, high saturation changes near the surface, immediately after rainfall, can impact the dV/V because of the 8-Hz R-wave sensitivity between 0 and 10 m (Fig. 4c). The dV/V fast decreases were reproduced for the events of November 2014 (200 mm) and September 2015 (140 mm). The global shape of dV/V is well reproduced, even if the minimum computed dV/V is a few weeks in advance. This dephasing could be due to the model and the simplification of the bottom outlet to a constant flux of 1 mm d^{-1}. Another possibility is some hysteresis effect, already described on the site by Tritz et al. (2011). One can finally note that including dV/V in the model optimization did not significantly decrease the fit for simulated gravity or MRS water content, which shows the consistency of the different geophysical methods (Fig. 6).

Discussion

Parameter Constraint and Benefits from Relative Seismic Velocity Variations

Figure 7 shows the parameter constraint depending on which dataset was taken into account in the model optimization. The first layer (0–5 m) shows a very strong tradeoff between K_{s1} and n_1 (Fig. 7a). This layer was essentially constrained by gravity and actual evaporation, and the poor parameter constraint did not improve with MRS or seismic assimilation (not shown). A better constraint of this first layer could be achieved with, e.g., soil moisture probe information, but constraining the first meters is quite classical and out of the scope of this study, focusing on deep and inaccessible media.

On the contrary, parameters n_2 and K_{s2} of the second layer are not constrained at all by using only gravity and AET (Fig. 7b). The AET reproduction from PET depends only on water availability near the surface (then in Layer 1) and gravity depends on all the water, no matter where it is. When MRS is added to gravity and AET for parameter identification (i.e., we also reproduced the mean water content of 8% between 20 and 40 m), K_{s2} and n_2 were more constrained. A high-KGE area in parameter space is clearly defined even if the ranges of the parameters are not reduced and is still over several orders of magnitude (Fig. 7c). Finally, when dV/V is also assimilated, this area is largely reduced (Fig. 7d), with K_{s2} around tens to hundreds of centimeters per day and n_2 between 1.2 and 1.5. A trade-off still exists and may be due to the fact that we do not reproduce the amplitude of dV/V.

Our study is in line with many previous studies showing difficulties when using gravity alone to constrain hydrological models. For

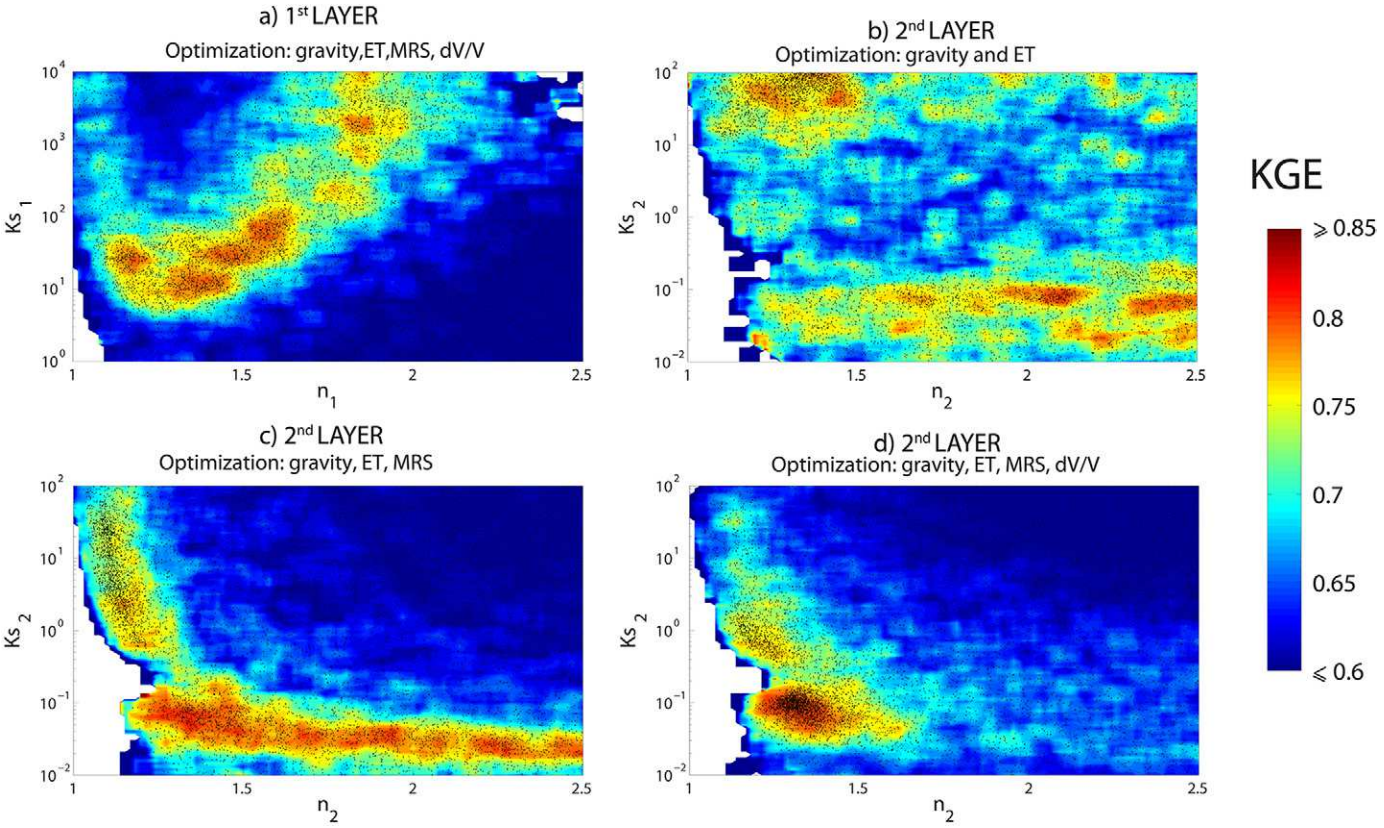

Fig. 7. Sensitivity of the parameter saturated hydraulic conductivity (K_s) and the shape parameter n, where each dot represents one model and the color represents the quality of the fit, evaluated with the Kling–Gupta efficiency (KGE) (the higher the value the better the fit) and averaged on cells with sides of 100th the size of the axis: (a) parameters of the first layer, optimization on all datasets (actual evapotranspiration [AET], gravity, relative seismic velocity variation [dV/V], and magnetic resonance sounding [MRS] water content); (b) parameters of the second layer, optimization on AET and gravity only; (c) parameters of the second layer, optimization on AET, gravity, and MRS water content; and (d) parameters of the second layer, optimization on AET, gravity, MRS water content, and dV/V at 6 to 8 Hz. Note the dense neighborhood sampling on high-KGE areas.

example, Blainey et al. (2007) did not constrain hydraulic parameters with gravity during a pumping test but found benefits when gravity was added to drawdown measurements. In a pumping test with synthetic data, Herckenrath et al. (2012) showed only a very small reduction in parameter uncertainty when adding gravity data and were skeptical about the usefulness of gravity under real conditions. However, Christiansen et al. (2011) used gravity with success on a vadose zone to constrain the van Genuchten K_s and n parameters in a synthetic case as well as in a forced infiltration experiment. More recently, Kennedy et al. (2014) have shown good results on a thick vadose zone using several gravimeters—including a superconducting gravimeter—during a controlled recharge. Most of those studies have been synthetic or under controlled conditions. In the case of this study, we faced natural conditions on a medium locally too heterogeneous to use boreholes; complementary information and complementary datasets were needed to constrain the hydraulic parameters.

We adopted here a coupled hydrogeophysical approach (e.g., Ferré et al., 2006), as geophysical responses (dV/V and gravity changes) are calculated at each step of the inversion process from the predicted hydrological response (HYDRUS-1D model). Simulated geophysical responses are directly compared with the observed data, and a single objective function is minimized that comprises all the observations. Different inversion approaches exist (e.g., Herckenrath et al., 2013; Hinnell et al., 2010), but we did not compare them in this preliminary study. We have a too-simplified model and we lack high-quality petrophysical relationships between S and dV/V on this karst. The comparison of different approaches in term of parameter uncertainty reduction should be conducted first on synthetic data, for known HYDRUS parameters, and coupling several dV/V at different frequencies (different depth sensitivities).

Petrophysical Relation between R-Wave Velocity and Saturation

Because of the karstic nature of the aquifer, this study faced particular problems, and the Biot–Gassmann relations, successfully implemented in porous media (Voisin et al., 2016), do not explain the amplitude here. However, the fact that we were not able to reproduce the amplitude of the observed dV/V raises major conceptual problems. Of course, the one-dimensional model is very simplistic, with a constant outlet and only two layers, but here we discuss some other reasons for this "petrophysical problem": the carbonated nature of the matrix; the assumption that V_P changes are negligible; and the assumption that the ambient noise source is temporally stable.

1. Biot–Gassmann relations assume that there are no interactions between the rock frame and the fluid fraction. This is unlikely in a karst environment, and numerous researchers have seen smaller S-wave velocities when saturating carbonates than those predicted by Biot–Gassmann theory (e.g., Cadoret, 1993; Vanorio et al., 2008). The reasons given are the dissolution of cement, disruption of cohesive forces, and an increase in porosity. On the same dolostones, Galibert (2016) needed to introduce a chemical factor to explain V_P and V_S changes obtained from time-lapse refraction seismic monitoring. However, electrical conductivity was monitored by probes in boreholes and did not show significant changes, which would indicate no dissolution. But once again, data from boreholes are representative of a much smaller scale than the geophysical experiments presented in this study.
2. The relation between saturation and P-wave velocity raises issues that were not discussed in this study. For the same amount of variation, V_P impacts R-waves less than V_S (about one order of magnitude less). However, P-waves are susceptible to showing much larger variations with saturation changes. If seismic wavelengths are smaller than the size of the heterogeneities, we can observe a "patchy saturation" effect (Knight et al., 1998). This is expressed by a continuous and strong increase of V_P with saturation. At the active seismic high frequencies, patchy saturation was observed by Galibert (2016) for some levels of the Durzon dolostones. In this study, we have supposed that we work at large enough wavelengths to mitigate small-scale heterogeneities ($\sim$150 m for 8-Hz noise and a 1000 m s^{-1} medium) and then that we do not observe patchy saturation. Otherwise, saturation would increase V_P (contrary to Vs, which decreases). Taking V_P increase into account would reduce the simulated R-wave dV/V, whereas it is already too small. If seismic wavelengths are larger than the size of the heterogeneities, which is our assumption, the medium can be considered homogeneous. The V_P shows a slight linear decrease (the same density effect as for V_S) until the very last percent of saturation, for which V_P strongly increases (Reuss, 1929). Then we can assume, for the same reason as above, that the medium is mainly unsaturated at the investigated depths. Otherwise, the large increase of V_P would reduce the dV/V decrease.
3. We assumed from the beginning that the road traffic is statically a stable source averaging across a day (Mainsant et al., 2012). However, our complex karstic site may be anisotropic due to fractures and alteration along them. The water content of fractures depends on the season and the amount of precipitation. If anisotropy is time dependent (depending on water content), it may virtually change the source position and invalidate the method. Then the signal may be still hydrologically induced, but also because of ray travel changes instead of pure V_R changes. Some observations are going in this way, as the different orientations of the noise depending on the frequency (Fig. 3c), or an orientation change after the November 2014 event at 10 to 15 Hz (not shown). Anisotropy at the observatory is a very interesting topic, but we obviously need more than two stations to study it.

Conclusions and Perspectives

We do observe a hydrological signal at the field scale (a few hundred meters) by correlating traffic seismic noise in the 6- to 8-Hz band between two seismic stations. The observed velocity decreased after rainfall, which implies that saturation has increased at sensitive depths (20–60 m for 6–8-Hz noise). It reveals a slow infiltration rate and a large unsaturated thickness beneath the observatory. Although boreholes indicate strong heterogeneity, modeling has shown the consistency of seismic data with other datasets and has validated the use of an equivalent one-dimensional model at the field scale on this specific site.

Gravimetry, MRS, and passive seismic appear to be complementary, with gravimetry constraining the water storage variations, MRS the mean vertical distribution of groundwater, and passive seismic giving a depth constraint in a one-dimensional profile. Indeed, the gravity signal changes only as water is added to or removed from the system but does not change as water moves vertically when the infinite slab approximation is used. In contrast, the seismic signal changes as water moves through the vadose zone because a given frequency has a defined depth sensitivity profile. Moreover, gravimetry, passive seismic, and MRS are all noninvasive methods and they all have a comparable investigation scale: a radius of hundreds of meters for the gravimeter and MRS and an inter-station distance of 400 m for the ambient seismic noise with large enough wavelengths to mitigate small-scale heterogeneities. Ambient seismic noise should be also applicable on various aquifers (classic porous media) where shallow or destructive methods are not suited or it is not possible to use them. It should be also applicable at various spatial scales, for example with satellite gravimetry in continental-scale models using large permanent seismic networks.

Passive seismic monitoring for the identification of hydrological parameters needs geological a priori information and a V_S reference profile to define the depth sensitivity, and it is not straightforward on karst. Nonetheless, we showed the benefit of dV/V for constraining hydrological parameters with only one frequency band (6–8 Hz), a simplified V_S profile, and a hydrological model. Thus the method demonstrates great potential for the study of deep critical zones. Future works should be conducted on other sites where hydraulic parameters are better known, or on synthetic data, to study the accuracy of parameters retrieved from dV/V and their uncertainty.

On the observatory karstic site, we lacked a high-quality petrophysical relationship and we were not able to reproduce the observed dV/V amplitude using the Biot–Gassmann theory. A linear relation between saturation and V_S allows a good reproduction of the observed dV/V at 6 to 8 Hz at the first order, but as long as the linear coefficient is unknown, we lose potential information on porosity and model geometry. More realistic models (geometry, additional layers and parameters) could be researched with more dV/V signals available at different frequencies. Nonetheless it will not solve the petrophysics problem. Several tracks are being studied such as the dissolution–precipitation effect or saturation-dependent anisotropy. Ten seismic stations will be deployed soon on the Durzon basin. More pairs of seismometers should ensure more accurate dV/V, and the azimuth coverage would allow investigation of anisotropy changes. One last possibility may be that the signal does not come from saturation changes but from pressure changes in fractures. An unfractured site should be studied as well as a karstic site, where fast transfer through fractures dominates and where pressure changes in fractures are proven (Lesparre et al., 2016).

Acknowledgments

We thank the Region Languedoc-Roussillon, the OSU OREME observatory and the National observation system (SNO) H+, which is a part of OZCAR, the French network of Critical Zone Observatories. The data were acquired using instruments belonging to the French national pool of portable seismic stations and gravimeters RESIF SISMOB and GMOB. The RESIF is a national research infrastructure, recognized as such by the French Ministry of Higher Education and Research. The RESIF is managed by the RESIF Consortium, composed of 18 research institutions and universities in France. The RESIF is additionally supported by a public grant overseen by the French National Research Agency (ANR) as part of the "Investissements d'Avenir" program (reference: ANR-11-EQPX-0040) and the French Ministry of Ecology, Sustainable Development and Energy. We are grateful to Nicolas Le Moigne for the superconducting gravimeter time series. Observatory data (gravity, meteorological, seismic) are available on OSU OREME and SNO H+ websites (http://data.oreme.org/gek/home; http://hplus.ore.fr). We also thank two anonymous reviewers for their valuable remarks.

References

Adelinet, M., C. Domínguez, J. Fortin, and S. Violette. 2018. Seismic-refraction field experiments on Galapagos Islands: A quantitative tool for hydrogeology. J. Appl. Geophys. 148:139–151. doi:10.1016/j.jappgeo.2017.10.009

Biot, M.A. 1956a. Theory of propagation of elastic waves in a fluid-saturated porous solid: I. Low-frequency range. J. Acoust. Soc. Am. 28:168–178. doi:10.1121/1.1908239

Biot, M.A. 1956b. Theory of propagation of elastic waves in a fluid-saturated porous solid: II. Higher frequency range. J. Acoust. Soc. Am. 28:179–191. doi:10.1121/1.1908241

Blainey, J.B., T.P.A. Ferré, and J.T. Cordova. 2007. Assessing the likely value of gravity and drawdown measurements to constrain estimates of hydraulic conductivity and specific yield during unconfined aquifer testing. Water Resour. Res. 43:W12408. doi:10.1029/2006WR005678

Bottelin, P., D. Jongmans, L. Baillet, T. Lebourg, D. Hantz, C. Lévy, and J. Turpin. 2013. Spectral analysis of prone-to-fall rock compartments using ambient vibrations. J. Environ. Eng. Geophys. 18:205–217. doi:10.2113/JEEG18.4.205

Brantley, S.L., W.E. Dietrich, and S. Banwart. 2015. An international initiative for science in the critical zone. EOS 96. doi:10.1029/2015EO031111

Brenguier, F., M. Campillo, C. Hadziioannou, N. Shapiro, R. Nadeau, and E. Larose. 2008a. Postseismic relaxation along the San Andreas fault at Parkfield from continuous seismological observations. Science 321:1478–1481. doi:10.1126/science.1160943

Brenguier, F., N.M. Shapiro, M. Campillo, V. Ferrazzini, Z. Duputel, O. Coutant, and A. Nercessian. 2008b. Towards forecasting volcanic eruptions using seismic noise. Nat. Geosci. 1:126–130. doi:10.1038/ngeo104

Cadoret, T. 1993. Effet de la saturation eau-gaz sur les propriétés acoustiques des roches. Etude aux fréquences sonores et ultrasonores. Ph.D. diss. Université Paris Diderot, Paris.

Campillo, M., and A. Paul. 2003. Long-range correlations in the diffuse seismic coda. Science 299:547–549. doi:10.1126/science.1078551

Chalikakis, K., V. Plagnes, R. Guerin, R. Valois, and F.P. Bosch. 2011. Contribution of geophysical methods to karst-system exploration: An overview. Hydrogeol. J. 19:1169–1180. doi:10.1007/s10040-011-0746-x

Christiansen, L., E.B. Haarder, A.B. Hansen, M.C. Looms, P.J. Binning, D. Rosbjerg, and P. Bauer-Gottwein. 2011. Calibrating vadose zone models with time-lapse gravity data. Vadose Zone J. 10:1034–1044. doi:10.2136/vzj2010.0127

Clarke, D., L. Zaccarelli, N.M. Shapiro, and F. Brenguier. 2011. Assessment of resolution and accuracy of the moving window cross spectral technique for monitoring crustal temporal variations using ambient seismic noise. Geophys. J. Int. 186:867–882. doi:10.1111/j.1365-246X.2011.05074.x

Deville, S., T. Jacob, J. Chéry, and C. Champollion. 2012. On the impact of topography and building mask on time varying gravity due to local hydrology. Geophys. J. Int.192:82–93. doi:10.1093/gji/ggs007

Ferré, T.P.A., A.C. Hinnell, and J.B. Blainey. 2006. Inferring hydraulic properties using surface-based electrical resistivity during infiltration. Leading Edge 25:720–723. doi:10.1190/1.2210055

Fores, B., C. Champollion, N. Le Moigne, R. Bayer, and J. Chéry. 2017a. Assessing the precision of the iGrav superconducting gravimeter for hydrological models and karstic hydrological process identification. Geophys. J. Int. 208:269–280. doi:10.1093/gji/ggw396

Fores, B., C. Champollion, N. Le Moigne, and J. Chéry. 2017b. Impact of ambient temperature on spring-based relative gravimeter measurements. J. Geod. 91:269–277. doi:10.1007/s00190-016-0961-2

Galibert, P.Y. 2016. Quantitative estimation of water storage and residence time in the epikarst with time-lapse refraction seismic. Geophys. Prospect. 64:431–444. doi:10.1111/1365-2478.12272

Gassmann, F. 1951. Über die elastizität poröser medien. Vierteljahrsschr. Naturforsch. Ges. Zuerich 96:1–23.

Güntner, A., M. Reich, M. Mikolaj, B. Creutzfeldt, S. Schroeder, and H. Wziontek. 2017. Landscape-scale water balance monitoring with an iGrav superconducting gravimeter in a field enclosure. Hydrol. Earth Syst. Sci. 21:3167–3182. doi:10.5194/hess-21-3167-2017

Gupta, H.V., H. Kling, K.K. Yilmaz, and G.F. Martinez. 2009. Decomposition of the mean squared error and NSE performance criteria: Implications for improving hydrological modelling. J. Hydrol. 377:80–91. doi:10.1016/j.jhydrol.2009.08.003

Hadziioannou, C., E. Larose, O. Coutant, P. Roux, and M. Campillo. 2009. Stability of monitoring weak changes in multiply scattering media with ambient noise correlation: Laboratory experiments. J. Acoust. Soc. Am. 125:3688–3695. doi:10.1121/1.3125345

Hinderer, J., N. Florsch, J. Mäkinen, H. Legros, and J.E. Faller. 1991. On the calibration of a superconducting gravimeter using absolute gravity measurements. Geophys. J. Int. 106:491–497. doi:10.1111/j.1365-246X.1991.tb03907.x

Hinnell, A.C., T.P.A. Ferré, J.A. Vrugt, J.A. Huisman, S. Moysey, J. Rings, and M.B. Kowalsky. 2010. Improved extraction of hydrologic information from geophysical data through coupled hydrogeophysical inversion. Water Resour. Res. 46:W00D40. doi:10.1029/2008WR007060

Herckenrath, D., E. Auken, L. Christiansen, A.A. Behroozmand, and P. Bauer-Gottwein. 2012. Coupled hydrogeophysical inversion using time-lapse magnetic resonance sounding and time-lapse gravity data for hydraulic aquifer testing: Will it work in practice? Water Resour. Res. 48:W01539. doi:10.1029/2011WR010411

Herckenrath, D., G. Fiandaca, E. Auken, and P. Bauer-Gottwein. 2013. Sequential and joint hydrogeophysical inversion using a field-scale groundwater model with ERT and TDEM data. Hydrol. Earth Syst. Sci. 17:4043–4060. doi:10.5194/hess-17-4043-2013

Herrmann, R.B. 2013. Computer programs in seismology: An evolving tool for instruction and research. Seismol. Res. Lett. 84:1081–1088. doi:10.1785/0220110096

Jacob, T., R. Bayer, J. Chery, H. Jourde, N. Le Moigne, J.P. Boy, and P. Brunet. 2008. Absolute gravity monitoring of water storage variation in a karst aquifer on the Larzac Plateau (southern France). J. Hydrol. 359:105–117. doi:10.1016/j.jhydrol.2008.06.020

Jacob, T., J. Chery, R. Bayer, N. Le Moigne, J.P. Boy, P. Vernant, and F. Boudin. 2009. Time-lapse surface to depth gravity measurements on a karst system reveal the dominant role of the epikarst as a water storage entity. Geophys. J. Int. 177:347–360. doi:10.1111/j.1365-246X.2009.04118.x

Jazayeri Noushabadi, M.R., H. Jourde, and G. Massonnat. 2011. Influence of the observation scale on permeability estimation at local and regional scales through well tests in a fractured and karstic aquifer (Lez aquifer, southern France). J. Hydrol. 403:321–336. doi:10.1016/j.jhydrol.2011.04.013

Kennedy, J.R., T.P.A. Ferré, A. Guntner, M. Abe, and B. Creutzfeldt. 2014. Direct measurement of subsurface mass change using the variable baseline gravity gradient method. Geophys. Res. Lett. 41:2827–2834. doi:10.1002/2014GL059673

Knight, R., J. Dvorkin, and A. Nur. 1998. Acoustic signatures of partial saturation. Geophysics 63:132–138. doi:10.1190/1.1444305

Lecocq, T., C. Caudron, and F. Brenguier. 2014. MSNoise, a Python package for monitoring seismic velocity changes using ambient seismic noise. Seismol. Res. Lett. 85:715–726. doi:10.1785/0220130073

Lecocq, T., L. Longuevergne, H.A. Pedersen, F. Brenguier, and K. Stammler. 2017. Monitoring ground water storage at mesoscale using seismic noise: 30 years of continuous observation and thermo-elastic and hydrological modeling. Sci. Rep. 7:14241. doi:10.1038/s41598-017-14468-9

Legchenko, A., and P. Valla. 2002. A review of the basic principles for proton magnetic resonance sounding measurements. J. Appl. Geophys. 50:3–19. doi:10.1016/S0926-9851(02)00127-1

Lesparre, N., F. Boudin, C. Champollion, J. Chéry, C. Danquigny, H.C. Seat, and L. Longuevergne. 2016. New insights on fractures deformation from tiltmeter data measured inside the Fontaine de Vaucluse karst system. Geophys. J. Int. 208:1389–1402. doi:10.1093/gji/ggw446

Mainsant, G., E. Larose, C. Brönnimann, D. Jongmans, C. Michoud, and M. Jaboyedoff. 2012. Ambient seismic noise monitoring of a clay landslide: Toward failure prediction. J. Geophys. Res. 117:F01030. doi:10.1029/2011JF002159

Mazzilli, N., M. Boucher, K. Chalikakis, A. Legchenko, H. Jourde, and C. Champollion. 2016. Contribution of magnetic resonance soundings for characterizing water storage in the unsaturated zone of karst aquifers. Geophysics 81(4):WB49–WB61. doi:10.1190/geo2015-0411.1

Mualem, Y. 1976. A new model for predicting the hydraulic conductivity of unsaturated porous media. Water Resour. Res. 12:513–522. doi:10.1029/WR012i003p00513

Pasquet, S., L. Bodet, P. Bergamo, R. Guérin, R. Martin, R. Mourgues, and V. Tournat. 2016a. Small-scale seismic monitoring of varying water levels in granular media. Vadose Zone J. 15(7). doi:10.2136/vzj2015.11.0142

Pasquet, S., L. Bodet, A. Dhemaied, A. Mouhri, Q. Vitale, F. Rejiba, et al. 2015. Detecting different water table levels in a shallow aquifer with combined P-, surface and SH-wave surveys: Insights from V_P/V_S or Poisson's ratios. J. Appl. Geophys. 113:38–50. doi:10.1016/j.jappgeo.2014.12.005

Pasquet, S., W.S. Holbrook, B.J. Carr, and K.W.W. Sims. 2016b. Geophysical imaging of shallow degassing in a Yellowstone hydrothermal system. Geophys. Res. Lett. 43:12027–12035. doi:10.1002/2016GL071306

Poupinet, G., W.L. Ellsworth, and J. Frechet. 1984. Monitoring velocity variations in the crust using earthquake doublets: An application to the Calaveras Fault, California. J. Geophys. Res. 89(B7):5719–5731. doi:10.1029/JB089iB07p05719

Pfeffer, J., C. Champollion, G. Favreau, B. Cappelaere, J. Hinderer, M. Boucher, and O. Robert. 2013. Evaluating surface and subsurface water storage variations at small time and space scales from relative gravity measurements in semiarid Niger. Water Resour. Res. 49:3276–3291. doi:10.1002/wrcr.20235

Ratdomopurbo, A., and G. Poupinet. 1995. Monitoring a temporal change of seismic velocity in a volcano: Application to the 1992 eruption of Mt. Merapi (Indonesia). Geophys. Res. Lett. 22:775–778. doi:10.1029/95GL00302

Reuss, A. 1929. Berechnung der fliessgrense von mishkristallen. Z. Angew. Math. Mech. 9:49–58. doi:10.1002/zamm.19290090104

Richards, L.A. 1931. Capillary conduction of liquids through porous mediums. J. Appl. Phys. 1:318–333.

Sambridge, M. 1999. Geophysical inversion with a neighbourhood algorithm: I. Searching a parameter space. Geophys. J. Int. 138:479–494. doi:10.1046/j.1365-246X.1999.00876.x

Sens-Schönfelder, C., and U. Wegler. 2006. Passive image interferometry and seasonal variations of seismic velocities at Merapi Volcano, Indonesia. Geophys. Res. Lett. 33:L21302. doi:10.1029/2006GL027797

Šimůnek, J., M. Šejna, H. Saito, M. Sakai, and M.Th. van Genuchten. 2008. The HYDRUS-1D software package for simulating the movement of water, heat, and multiple solutes in variably saturated media. Version 4.0. HYDRUS Softw. Ser. 3. Dep. of Environ. Sci., Univ. of California, Riverside, CA.

Šimůnek, J., M.Th. van Genuchten, and M. Šejna. 2016. Recent developments and applications of the HYDRUS computer software packages. Vadose Zone J. 15(7). doi:10.2136/vzj2016.04.0033

Snieder, R., A. Grêt, H. Douma, and J. Scales. 2002. Coda wave interferometry for estimating nonlinear behavior in seismic velocity. Science 295:2253–2255. doi:10.1126/science.1070015

Tritz, S., V. Guinot, and H. Jourde. 2011. Modelling the behaviour of a karst system catchment using non-linear hysteretic conceptual model. J. Hydrol. 397:250–262. doi:10.1016/j.jhydrol.2010.12.001

van Genuchten, M.Th. 1980. A closed-form equation for predicting the hydraulic conductivity of unsaturated soils. Soil Sci. Soc. Am. J. 44:892–898. doi:10.2136/sssaj1980.03615995004400050002x

Vanorio, T., C. Scotellaro, and G. Mavko. 2008. The effect of chemical and physical processes on the acoustic properties of carbonate rocks. Leading Edge 27:1040–1048. doi:10.1190/1.2967558

Voisin, C., S. Garambois, C. Massey, and R. Brossier. 2016. Seismic noise monitoring of the water table in a deep-seated, slow-moving landslide. Interpretation 4(3):SJ67–SJ76. doi:10.1190/INT-2016-0010.1

Weaver, R., and O. Lobkis. 2001. Ultrasonics without a source: Thermal fluctuation correlations at MHz frequencies. Phys. Rev. Lett. 87:134301.

Williams, P.W. 2008. The role of the epikarst in karst and cave hydrogeology: A review. Int. J. Speleol. 37:1–10. doi:10.5038/1827-806X.37.1.1